Journal of
Materials Chemistry B

Materials for biology and medicine

Accepted Manuscript

This article can be cited before page numbers have been issued, to do this please use: M. Zhao, S. Wan, X. Peng, B. Zhang, Q. Pan, S. Li, B. He and Y. Pu, *J. Mater. Chem. B*, 2020, DOI: 10.1039/C9TB02400J.

ROYAL SOCIETY OF CHEMISTRY

rsc.li/materials-b

View Article Online
DOI: 10.1039/C9TB02400J

Journal Name

ARTICLE

Leveraging a polycationic polymer to direct tunable loading of anticancer agent and photosensitizer with opposite charges for chemo-photodynamic therapy

Received 00th January 20xx,
Accepted 00th January 20xx

DOI: 10.1039/x0xx00000x

www.rsc.org/

Mingying Zhao[a], Shiyu Wan[a], Xinyu Peng[b], Boya Zhang[b], Qingqing Pan[b], Sai Li[a*], Bin He[b], and Yuji Pu[b*]

Herein, we ported a primary containing polycationic polymer to load oppositely-charged anticancer drug (doxorubicin, DOX) and photosensitizer (chlorin e6, Ce6) for combinational chemo-photodynamic therapy. The electrostatic interactions as well as other multiple interactions between polymer and payloads rendered the drug-loaded nanoparticles excellent stability. Moreover, the electrostatic attraction between cationic polymer and anionic Ce6 dictated that Ce6 had higher loading efficiency than DOX. DOX showed a pH-responsive drug release owing to the elevated solubility of protonated DOX and reduced interaction with partially protonated polymer in acidic condition. In contrast, Ce6 showed pH-insensitive release because of the less change of solubility and the intense interactions between Ce6 and polymer. Synergistic chemo/photodynamic therapy of 4T1 cancer cells was achieved by light-triggered reactive oxygen species (ROS)-mediated enhanced cellular uptake and effective endo/lysosomal escape of drug-loaded nanoparticles. Our study demonstrated that the polycationic polymers could act as a robust polymer carrier for differential loading and release of oppositely-charged cargos for a combinational therapy.

Introduction

Chemotherapy is one of the main strategies for clinical treatment of cancer. However, the chemotherapeutics' poor killing selectivity between cancer and normal cells inevitably leads to severe systemic toxicity in chemotherapy.[1] Photodynamic therapy (PDT), another approved cancer treatment modality, kills cancer cells by reactive oxygen species (ROS) generated from photosensitizers (PSs) after light irradiation and has garnered much attention due to the inherent noninvasive and spatiotemporally controllable nature.[2, 3] Owing to the different anticancer mechanisms of chemotherapy and PDT, the chemo-photodynamic combination therapy has emerged as a strategy of great potential in efficiently ablating tumors and alleviating systemic toxicity caused by traditional chemotherapy.[4-6] However, the small and hydrophobic nature of most of the chemotherapeutics and PSs has severely limited their bioavailability for the insolubility in water.

Inspired by the hydrophobic nature of chemotherapeutics and PSs, various drug delivery systems (DDSs) have been developed to encapsulate chemotherapeutics and/or PSs by hydrophobic interactions, improving the anticancer efficacy and reducing side effects.[7-12] However, many anticancer drugs and photosensitizers also have amine and/or carboxylic groups, which are partly positively and negatively charged in neutral pH. For example, doxorubicin (DOX) and chlorin e6 (Ce6) are a typical anticancer drug and PS, respectively. They are both hydrophobic because of the aromatic structure; meanwhile, DOX and Ce6 have amine and carboxylic groups, respectively. In a typical DDS, DOX and Ce6 could be simultaneously loaded into an amphiphilic block copolymer with no charge to generate polymeric nanoparticles.[13-18] Recently, Zhang et al. reported that DOX and Ce6 could be directly used to construct carrier-free nanoparticles by the multiple interactions between DOX and Ce6 for chemo-photodynamic therapy.[19] Such nanodrugs could exhibit very high drug encapsulation efficiency and drug feeding molar ratio-dependent sizes. However, DOX and Ce6 showed comparable and relatively rapid drug release behaviors (about 60%–80% DOX and Ce6 were released within 48 h), which might lead to potential drug leakage in blood circulation and thereby systemic toxicity.

Polycationic polymers, natural or synthetic, have recently attracted wide attention and widely applied in many biomedical fields. For example, many natural antimicrobial peptides, widely existed in human, animals, and plants, are cationic in charge.[20] Many synthetic cationic polymers, such as those based on chitosan[21, 22], poly(meth)acrylates[23, 24], and polycarbonates[25, 26], and cationic polypeptides[27-29] and nylon-3 polymers[30, 31], etc., exhibited excellent, sometimes broad spectrum, antimicrobial activity. Meanwhile, polycationic polymers were widely used as

[a] School of Chemical Engineering, Sichuan University, Chengdu 610065, China
[b] National Engineering Research Center for Biomaterials, Sichuan University, Chengdu 610064, China
* Corresponding authors, E-mail: lisai@scu.edu.cn; yjpu@scu.edu.cn

† Electronic Supplementary Information (ESI) available: molecular property of mPEG-PC, DLS results and stability of nanoparticles, in vitro anticancer study and H&E images of main organs. See DOI: 10.1039/x0xx00000x

a virus mimicking carrier to condense and deliver negatively-charged, therapeutic genes to targeted (cancer) cells for gene therapy.[32, 33] Similarly, Kataoka et al developed polyion complex micelles (PIC), composed of cationic and anionic polymers, for efficiently loading and delivery of charged proteins and nucleic acids.[34-36] For example, they used poly(ethylene glycol)-*b*-poly(aspartic acid) and a porphyrin-cored third generation dendrimer decorated with 32 primary amine groups to prepare PS-loaded PICs for PDT of lung cancer.[37]

Herein, we reported a cationic polymer-based DDS for efficient co-loading of oppositely-charged drugs; cationic anticancer drug (DOX) and anionic PS (Ce6) were employed as model drugs to demonstrate the feasibility of this strategy. A block copolymer of methoxy polyethylene glycol (mPEG) and polycarbonates (PCs) (mPEG-PC, Scheme 2) was designed for the outstanding biocompatibility and biodegradability of PEG and PC.[17, 38-40] PC block was functionalized with primary amine groups to render the polymer cationic charges. DOX and Ce6 were efficiently loaded into the polymeric nanoparticles by multiple intermolecular interactions between polymer and payloads (Scheme 1). The impact of polymer-payload interactions on the drug loading efficiency, nanoparticle stability, and drug release behaviors were studied. The *in vitro* and *in vivo* combinational chemo-photodynamic therapy of murine breast cancer were further investigated to establish the anticancer efficiency of this DDS.

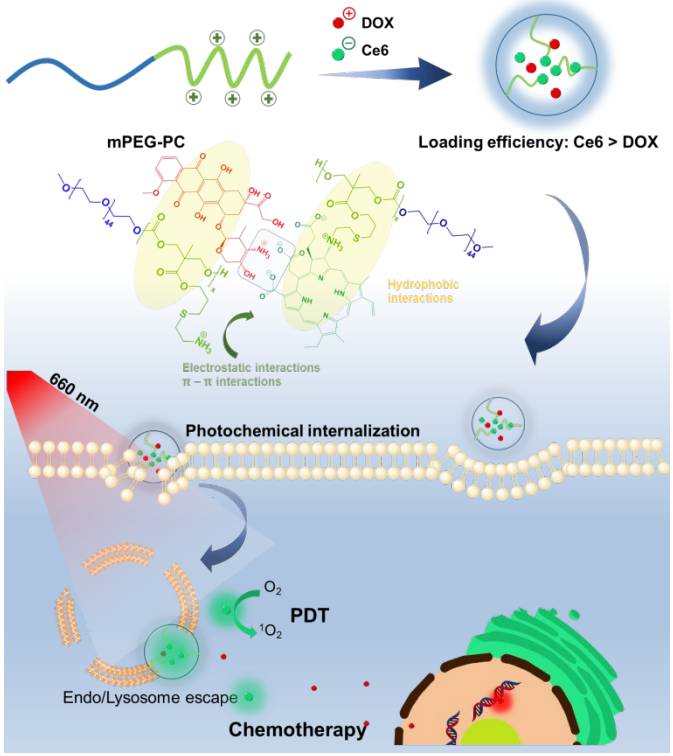

Scheme 1 Schematic illustration of utilization of cationic polymer, mPEG-PC, for differential loading of DOX and Ce6 and the combinational chemo/photodynamic therapy.

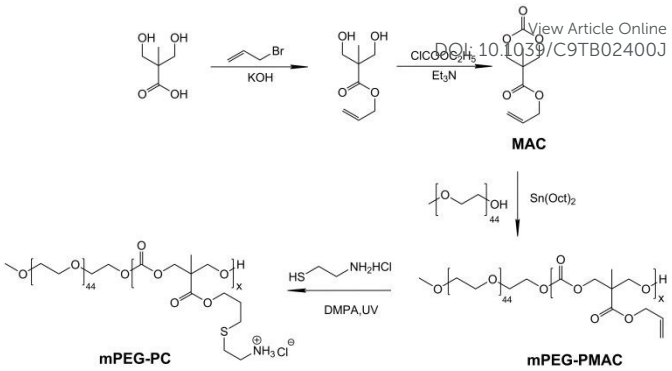

Scheme 2 The synthetic illustration of polycationic block copolymer mPEG-PC.

Experimental

Synthesis of mPEG-PC

The synthetic scheme of mPEG-PC is shown in Scheme 2.

Synthesis of 5-methyl-5-allyloxycarbonyl-propylene carbonate (MAC). The synthesis of MAC was according the previous work reported by Jing et al.[41] Firstly, 2,2-bis(hydroxymethyl)propionic acid (18.0 g, 134 mmol) and KOH (8.6 g, 153 mmol) were dissolved in 150 mL of DMF at 100 °C. Allyl bromide (11.6 mL, 134 mmol) was added dropwise and the mixture was stirred for 48 h at 45 °C. DMF was removed under vacuum and the residue was dissolved in 200 mL dichloromethane and extracted by deionized water (100 mL × 2). The organic phase was combined and dried with anhydrous Na_2SO_4. After removal of dichloromethane under vacuum, allyl 2,2-bis(hydroxymethyl)propionate was obtained with a yield of 56%. Secondly, allyl 2,2-bis(hydroxymethyl)propionate (14 g, 80 mmol) and $ClCO_2Et$ (22.86 mL, 240 mmol) were dissolved in 200 mL anhydrous tetrahydrofuran (THF). Triethylamine (33 mL, 0.24 mol) was added dropwise into the stirring mixture at 0 °C within 30 min. The mixture was then stirred at room temperature for 2 h. The precipitate was filtered off and THF was removed to obtain crude products, which were recrystallized from THF/ethyl ether for three times to give the white crystals MAC (yield：62%).

Synthesis of mPEG-PMAC. mPEG-PMAC was prepared via ring-opening polymerization of MAC using $mPEG_{2000}$ as a macro-initiator. Briefly, $mPEG_{2000}$ (0.3 g, 0.15 mmol) was added into the polymerization tube and stirred at 100 °C under vacuum for 2 h to remove trace water. MAC and $Sn(Oct)_2$ in dry toluene were added quickly into the cooled tube. After purged with nitrogen gas for three times, the tube was sealed and immersed in an oil bath at 110 °C for 24 h. The mixture was dissolved in DCM and precipitated into excessive cold diethyl ether to obtain mPEG-PMAC.

Synthesis of mPEG-PC. mPEG-PMAC (0.5 g, 1.14 mmol), cysteamine hydrochloride (772 mg, 6.80 mmol), and DMPA (69.7 mg, 0.272 mmol) were dissolved in 25 mL DMF under argon atmosphere. The mixture was stirred at room temperature under UV irradiation (365 nm) for 3 h. Afterwards, the mixture was dialyzed against deionized water in a dialysis

bag (MWCO 2000) for 2 d. The freeze-dried product was dissolved in methanol and then precipitated in diethyl ether. The precipitate was then dried in vacuum to obtain mPEG-PC.

Preparation and characterization of drug-loaded mPEG-PC nanoparticles

The drug-loaded mPEG-PC nanoparticles were prepared by nanoprecipitation. Different rations of Ce6 and DOX and mPEG-PC (10 mg) were dissolved in DMSO (1 mL), and the solution was ultrasonicated for 10 min. Thereafter, the solution was added dropwise into stirring deionized water (10 mL) and stirred overnight in the dark. After dialysis against deionized water in a dialysis bag (MWCO 1000) for 24 h, the mixture was centrifuged (3000 rpm, 5 min) to remove unloaded DOX and Ce6. The supernatant was freeze-dried to obtain mPEG-PC-Ce6-DOX nanoparticles (DNPs). The drug loading contents (DLCs) and drug loading efficiencies (DLEs) of Ce6 and DOX were determined by fluorescence spectroscopy at 687 and 585 nm (Hitachi F-7000), respectively.[42] The blank mPEG-PC nanoparticles were prepared similarly.

Stability of DNPs

DNPs solution containing 10% FBS was incubated in a shaking bed at 37 °C with a shaking rate of 150 rpm. The size changes of DNPs were monitored by DLS.

pH titration of mPEG-PC

The pH value of mPEG-PC solution (2 mg/mL) was adjusted to 10 by aqueous NaOH (0.2 mol/L). Aqueous HCl (0.01 mol/L) was added dropwise until the pH of mPEG-PC aqueous solution declined to 4.0.

***In vitro* drug release**

The release kinetic profiles of DOX and Ce6 from DNPs were measured by a dialysis method. Drug-loaded nanoparticles were dispersed in phosphate buffer solutions with different pH values (pH 7.4 and 5.0, 10 mM). The solutions were transferred into dialysis bags (MWCO 2000), which were immersed in 15 mL of buffer solution (containing 0.2% Tween 80) of different pH values in dark and incubated in a shaking bed at 37 °C with a shaking rate of 150 rpm. At predetermined time intervals, 1 mL of medium with released drug was taken out for measurement and 1 mL fresh medium was supplemented. The released Ce6 and DOX were respectively detected at 687 and 585 nm on a fluorescence spectrophotometer. For the drug release with the light irradiation, the protocol was similar except that the DNPs in dialysis bags were irradiated (660 nm, 3 min) at 4, 8, and 12 h. The released amount of Ce6 was measured similarly.

Singlet oxygen ($^1O_2$) detection by SOSG

DNPs were dispersed in PBS with different pH values to a concentration of 0.02 mg/mL. After a 6-h incubation in a shaking bed (150 rpm) at 37 °C. DNPs suspension (100 μL) was diluted to 1 mL by DI water. SOSG solution in DI water (containing 0.3% methanol, 50 μL) was added into the diluted DNPs suspension and the working concentration of SOSG was 1.5 μM. The fluorescence of the suspension at 525 nm was measured after light irradiation (λ = 660 nm) of 3, 8 or 13 min.

Cytotoxicity test

The cytotoxicity of mPEG-PC and DNPs against NIH/3T3 and/or 4T1 cells was measured by an MTT assay. Cells were seeded in 96-well plates (Corning Inc., New York) at a density of 8×10^3 NIH/3T3 cells/well or 4×10^3 4T1 cells/well and cultured for 24 h. Culture medium containing different concentrations of mPEG-PC or DNPs was then added. After 12 h，for the mPEG-PC cytotoxicity study, cells in the irradiation group were illuminated with a 660 nm light for 10 min. For the DNPs cytotoxicity study, cells in the irradiation groups were illuminated for 0.5, 1, and 3 min. Cells were then incubated for another 12 h. Thereafter, the medium was discarded and replaced with 100 μL of MTT in serum-free medium (0.5 mg/mL). After incubation for 4 h, medium was removed and 100 μL DMSO was added into each well. The absorbance at 490 nm was measured by a microplate reader. The cell viability was expressed as (sample/control) × 100%. All data were presented as mean ± SD (n = 3).

Cellular uptake

Cellular uptake in the dark. For cytometry, 4T1 cells were seeded in 6-well plates (1×10^5 cells/well) and cultured at 37 °C for 24 h. Cells were then treated with culture medium containing DNPs (DOX: 3 μg/mL) for 1, 2, and 4 h. After trypsinization and centrifugation (2500 rpm, 3 min), cells were rinsed with PBS twice and re-suspended in 350 μL PBS for study on a FACScan instrument (Becton Dickinson, Accuri C6). The DOX fluorescence was detected with excitation wavelength at 488 nm and emission wavelength at 585 nm. For CLSM study, 4T1 cells were seeded on 35 mm diameter glass dishes at a density of 2×10^4 cells/mL and cultured for 24 h. Cells were then treated with medium containing DNPs for 1, 2, and 4 h. Cells were stained with Hoechst for 20 min, washed, and immersed in PBS for CLSM observation. DOX and Hoechst were excited at 488 and 346 nm with emission at 585 and 460 nm, respectively.

Cellular uptake with light irradiation. 4T1 cells were seeded in 6-well plates (1×10^5 cells/well) and cultured for 24 h. Cells were then treated with culture medium containing DNPs (Ce6: 5 μg/mL) with or without light irradiation for 3 min and then cultured for 2 h. The following protocol was similar to that of the cellular uptake in the dark.

Intracellular drug release

4T1 cells were seeded on 35 mm diameter glass dishes and cultured for 24 h. Cells were then treated with DNPs containing medium (DOX: 3 μg/mL) for 0.5 h. The culture medium was replaced by fresh medium and cells were further incubated for 5 h. Dishes were rinsed with PBS for three times and immersed in 1 mL PBS for CLSM study.

Intracellular ROS detection

4T1 cells were seeded on 35 mm diameter glass dishes at a cell density of 2×10^4 cells/mL and cultured for 24 h. Cells were then treated with DNPs containing medium (DOX: 3 μg/mL) for 2 h. Culture medium was replaced by serum-free medium containing DCFH-DA (10 μM). After 20 min, cells were treated with or without light irradiation for 3 min. Dishes were rinsed with PBS for three times and immersed in 1 mL PBS for CLSM study. DCF was excited at 488 with emission at 525 nm.

For cytometry, 4T1 cells were seeded in 6-well plates (1×10^5 cells/well) and cultured for 24 h. Cells were then treated with

culture medium containing DNPs (DOX: 3 μg/mL) for 2 h. Culture medium was replaced by serum-free medium containing DCFH-DA (10 μM). After 20 min, cells were harvested and rinsed with PBS twice. Samples were finally re-suspended in 350 μL PBS and then irradiated for 0, 3, and 5 min. Cells treated with blank culture medium was used as a control. The fluorescence intensity of DCF in 4T1 cells was detected with excitation wavelength at 488 nm.

Subcellular localization

4T1 cells were seeded on 35 mm diameter glass dishes at a cell density of 2×10^4 cells/mL and cultured for 24 h. Cells were then incubated with DNPs containing medium (DOX: 3 μg/mL) for 2 h. The medium was replaced with fresh medium, and cells were then treated with or without irradiation for 30 s and then cultured for additional 1 h. Cells were stained with lysotracker for 30 min, rinsed with PBS for three times, and immersed in 1 mL PBS for CLSM test.

***Ex vivo* biodistribution**

Male Balb/c mice (6 weeks) were purchased from Dashuo Biotechnology Co. Ltd. (Chengdu, Sichuan). 4T1 cells (1×10^6) were injected into mice right flanks subcutaneously. Ce6+ DOX·HCl (Ce6 of 5 mg/kg; DOX·HCl of 3 mg/kg) and DNPs (equivalent Ce6 of 5 mg/kg; equivalent DOX of 3 mg/kg) were intravenously injected via tail vein when tumor volume reached about 200 mm^3. At predetermined times, mice were sacrificed, and the main organs and tumors were collected and imaged *ex vivo* by an in-vivo imaging system (Maestro).

***In vivo* antitumor study**

The *in vivo* studies were carried out in compliance with the Animal Management Rules of the Ministry of Health of the People's Republic of China (Document no. 55, 2001) and the institutional guidelines. The experiments were approved by the Animal Care and Use Committee of Sichuan University. 4T1 tumor-bearing mice were randomly divided into four groups (n = 5) when tumor volume reached 100-150 mm^3. Four kinds of formulations were administrated via tail intravenous injection on days 0, 3, and 6: (1) Saline; (2) Ce6 (5 mg/kg); (3) DOX·HCl (3 mg/kg); and (4) DNPs (equivalent Ce6 of 5 mg/kg; equivalent DOX of 3 mg/kg). For Ce6 and DNPs groups, tumor was irradiated (660 nm, 100 mW/cm^2, 10 min) 6 h post-injection. The tumor volumes and body weights of mice were measured every 2 days. After 12 days, mice were sacrificed. The main organs (heart, liver, spleen, lung, and kidney) and tumors were excised to fix in 4% paraformaldehyde and then stained for H&E studies.

Statistical analysis

Student t-test was used to conduct statistical analysis. Statistical significance was set at $*p < 0.05$, $** p < 0.01$, $*** p < 0.001$.

Results and discussion

Synthesis and characterization of mPEG-PC

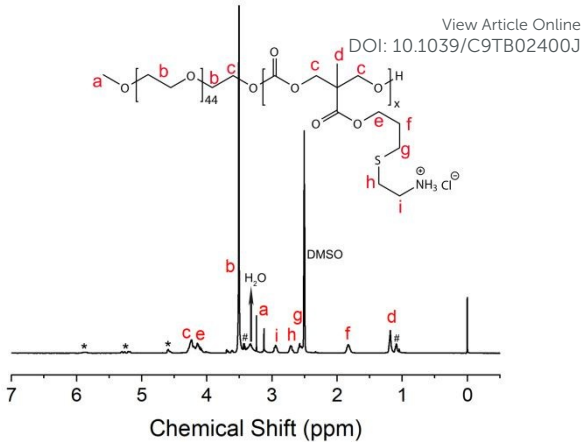

Fig. 1 ^{1}H NMR spectrum of mPEG-PC in DMSO-d_6. (* shows the residual peak of unmodified polymer side chains and # represents the residual peak of diethyl ether.)

Scheme 1 outlines the strategy of preparation of Ce6 and DOX co-loaded nanoparticles by supramolecular assembly of mPEG-PC, Ce6, and DOX. Structurally, photosensitizer Ce6 and chemotherapeutics DOX have hydrophobic and aromatic groups; besides, they have negative carboxylic groups and cationic amine groups, respectively. A polycationic block copolymer mPEG-*block*-polycarbonate, mPEG-PC, was used to co-load DOX and Ce6. The hydrophobic and cationic polycarbonate segments render strong intermolecular interactions between polymers and cargos including hydrophobic interactions, hydrogen bonding and electrostatic interactions (Scheme 1). Meanwhile, strong interactions between Ce6 and DOX, including electrostatic, π–π stacking and hydrophobic interactions, also favor the nanoparticle formation.[19]

The synthesis of mPEG-PC was illustrated in Scheme 2. Firstly, cyclic carbonate monomer MAC containing carbon-carbon double bond was synthesized *via* successive esterification and cyclization of 2,2-bis(hydroxymethyl)propionic acid. The chemical structure of MAC was verified by ^{1}H NMR (Fig. S1). mPEG-PMAC was then synthesized by ring opening polymerization of MAC using mPEG as macro-initiator and $Sn(Oct)_2$ as catalyst. The ^{1}H NMR spectrum of mPEG-PMAC was shown in Fig. S2; peaks f and b were ascribed to the allyl and methene protons in the polycarbonate and mPEG segments. The degree of polymerization was calculated to be 12 and the molecular weight of mPEG-PC was 4400 g/mol by NMR. Gel permeation chromatography (GPC) was studied to further confirm the successful polymerization; the number-average molecular weight of mPEG-PMAC was measured to be 8000 g/mol (Fig. S3 and Table S1).

mPEG-PC was then synthesized by thiol-ene click reactions between the thiols in cysteamine hydrochloride and the carbon-carbon double bonds in mPEG-PMAC (Scheme 2).[43] The successful synthesis of mPEG-PC was demonstrated by ^{1}H NMR (Fig. 1). The new peaks i (2.95–2.98 ppm) and h (2.68–2.72 ppm) corresponding to the methene protons of the pristine cysteamine appeared, suggesting successful chemical modification. The intensity of peaks at 5.81–5.91 ppm and

View Article Online
DOI: 10.1039/C9TB02400J

5.17–5.31 ppm that were ascribed to the allyl protons decreased sharply. The percentage of modification was calculated to be 85% by comparison of these peaks' areas.

Primary, secondary, and tertiary amine containing polymers can be protonated at acidic pH, for example in acidic organelles (endosomes and/or lysosomes), showing a pH-responsive property. To study the pH-responsiveness of mPEG-PC, we conducted an acid-base titration of mPEG-PC solution.[44] The pH-sensitive range of mPEG-PC was determined to be pH 8.4 to 4.9 by the first order derivation of the titration curve (Fig. S4).

Preparation and characterization of blank and drug-loaded polymeric nanoparticles

We then used mPEG-PC to prepare blank and drug-loaded NPs by adjusting the feeding weight ratios of Ce6 to DOX (Table 1, NP-1 to 5). The formation of nanoparticles was confirmed by the count rate results, which were obtained by dynamic light scattering (DLS) and summarized in Table 1. The blank polymeric NPs showed very low count rate (13 kcps), indicating its poor ability to generate nanoparticles, which was probably due to the low hydrophobicity of mPEG-PC. In contrast, DOX- and/or Ce6-loaded NPs showed much higher count rates (> 10 times), suggesting the successful nanoparticle formation. The multiple interactions including electrostatic interactions, hydrophobic, and π-π interactions between drugs and mPEG-PC collectively facilitated the nanoparticle preparation (Scheme 1). The NPs showed a diameter of tens of nanometers by DLS and positive zeta potentials in water. (Fig. S5 and Table 1).

Table 1 DLCs, DLEs, sizes, and zeta potentials of drug-loaded polymer nanoparticles.

Samples	Feeding weight ratio of Ce6 and DOX		DLCs (%)	DLEs (%)	Size[a] (nm)	Zeta potential[b] (mV)	Count rate[a] (kcps)
Blank	-		-	-	103.1	+22.4	13
NP-1	Ce6	0%	-	-	35.12	+26.7	148
	DOX	50%	14.0	28.0			
NP-2	Ce6	15%	7.0	46.7	25.65	+19.8	348
	DOX	35%	11.9	34.0			
NP-3 **(DNPs)**	Ce6	25%	13.8	55.2	33.90	+6.79	287
	DOX	25%	9.4	37.6			
NP-4	Ce6	35%	15.4	44.0	50.06	+5.89	256
	DOX	15%	5.3	35.3			
NP-5	Ce6	50%	16.4	32.8	39.56	+4.08	243
	DOX	0%	-	-			

a. The concentration of NPs was 0.4 mg/mL.

b. Tested in deionized water.

The NPs with higher loading capacity of DOX showed higher zeta potential owing to the positive charge nature of DOX. The successful loading of DOX and Ce6 was verified by UV absorption. As shown in Fig. 2A, the characteristic peaks of DOX and Ce6 at 480 and 411 nm appeared in the UV absorption of DNPs in DMSO. A red shift of these two peaks in the UV spectrum of DNPs in water was ascribed to the π-π interactions in the DNPs.[45, 46] The DOX and/or Ce6 loading efficiency and capacity by mPEG-PC were then studied by fluorescence spectroscopy (Fig. 2B).[19, 47-49] Free DOX and Ce6 emit strong fluorescence at 585 and 670 nm when excited at 480 and 400 nm, respectively (Fig. S6). Because dimethyl sulfoxide (DMSO) is a good solvent for both polymer and drugs, DMSO was used as solvent to disintegrate NPs and adequately dissolve free drugs for fluorescence study. As shown in Table 1, when the total feeding amount of DOX and Ce6 was fixed (50wt% in polymer + drug system), the DLCs would increase as the increase of the feeding ratio of drugs. NP-3 showed the highest total DLCs of 23.2% (13.8% and 9.4% for Ce6 and DOX, respectively). It should be noted that in all groups the DLEs of Ce6 were higher than those of DOX in the co-loaded NPs (NP-2, 3, and 4). The higher DLE of Ce6 was ascribed to the strong electrostatic attraction between negatively-charged Ce6 and positively-charged mPEG-PC. The electrostatic interactions were also confirmed by the zeta potential results (Table 1); the higher DLC of negatively-charged Ce6, the lower zeta potential of NPs in water. Furthermore, the hydrophobic interactions in DNPs were demonstrated by ^{1}H NMR.[50] As shown in Fig. S7, the peaks of DOX and Ce6 were not found in the ^{1}H NMR spectrum when D_2O was used as a solvent. In stark contrast, peaks of Ce6 and DOX at low field appeared when DMSO-d_6, a good solvent of polymer and drugs, was used. These NMR results verified that hydrophobic interactions were present in DNPs and DOX and Ce6 were mainly dispersed in the hydrophobic core.

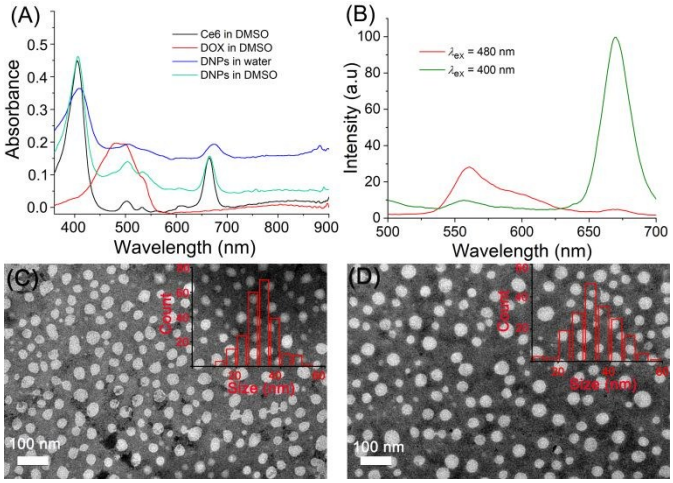

Fig. 2 UV absorption (A) and fluorescence spectroscopy (B, in DMSO) of DNPs. TEM images of DNPs in neutral (C) and acidic (D) environment for 4 h.

The stability of these NPs was studied by dilution (Fig. S5). DOX-loaded NP-1 and DOX and Ce6 co-loaded NP-2 showed a size change after dilution, suggesting a relatively weak stability. However, other co-loaded NPs (NP-3 and NP-4) and Ce6-loaded NPs (NP-5) showed better stability against dilution and no obvious size changes were observed after dilution, suggesting their more intense intermolecular interactions in these NPs. Considering the highest DLEs and that relatively low zeta potential is conductive to long blood circulation[51], we utilized the co-loaded NP-3 (denoted as DNPs) for the following study. The TEM image (Fig. 2C) manifested that DNPs were spherical with a diameter of about 30 nm, comparable with the DLS size (Table 1). The stability of DNPs in 10% FBS was also studied (Fig. S8). Negligible size changes were observed after a 24-h incubation, implying that DNPs could possess favorable stability in circulation.

In vitro drug release and singlet oxygen generation under light irradiation

The *in vitro* drug release behavior of DNPs was investigated in different pH conditions (PBS, pH 7.4 and 5.0. Fig. 3). DNPs showed comparable and slow release of Ce6 (< 40% at 48 h) in pH 7.4 and pH 5.0. However, the DOX release from DNPs was pH-responsive. The DNPs showed a sustained and minimal drug release in neutral pH condition; about 40% DOX was released within 48 h. However, a much faster release of DOX was observed at pH 5.0 and about 80% was released at 48 h. The different release behaviors of DOX and Ce6 from DNPs in different pH conditions were ascribed to their different solubility in acidic conditions and their distinct interactions with polymer carrier. In acidic condition, primary amine of DOX is protonated and the water solubility could be significantly improved, resulting into accelerated diffusion and drug release. In contrast, Ce6 showed slight slower release in acidic condition owing to the reduced solubility of carboxyl groups. Compared with the carrier-free nanodrugs,[19] DNPs showed much slower *in vitro* drug release, which was probably due to the protection of PEG shell and intense polymer-payloads interactions and conductive to the less drug leakage in blood circulation.

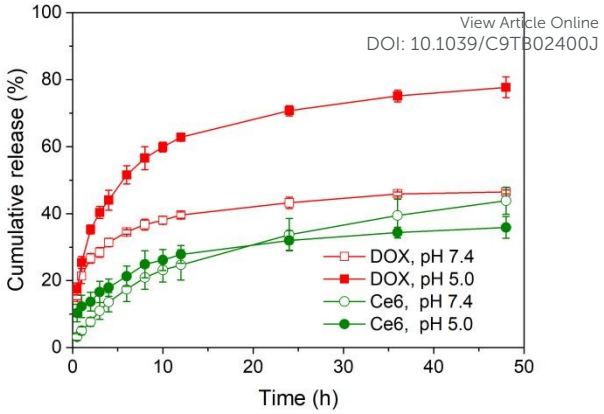

Fig. 3 *In vitro* drug release of DOX and Ce6 from DNPs in different pH conditions.

To further understand the underlying mechanism of differential drug release, we further studied the size and morphology of DNPs in acidic condition. As shown in Figure 2C and D, the DNPs in acidic condition showed comparable size with and similar morphology to that in neutral condition, suggesting that the nanoparticles were not rapidly disassociated by protonation of mPEG-PC. Thereafter, the zeta potentials of DNPs in different pH conditions were studied (Fig. S9). DNPs showed negative (−1.77 mV) and positive (+1.45 mV) zeta potentials in pH 8.4 and 5.0, respectively, indicating the protonation of mPEG-PC in acidic condition. Therefore, the acid-accelerated release of DOX could be partly ascribed to the electrostatic repulsion of positively-charged, protonated DOX and polymers.[45, 52] Given the low cationic charge and relatively stable nanoarchitecture of DNPs at pH 5, a rational explanation could be that mPEG-PC was partially protonated in acidic condition but the nanoparticles could be still stabilized by the intense interactions between mPEG-PC and Ce6.

The generation of singlet oxygen by DNPs in aqueous was then studied by using singlet oxygen sensor green (SOSG) as a fluorescence probe. DNPs were suspended in PBS (pH 7.4 and 5.0) for 6 h and then irradiated by laser light of 660 nm for different irradiation times. As shown in Fig. S10, DNPs in pH 5.0 generated more singlet oxygen than those in pH 7.4, which was probably due to easy diffusion of the generated singlet oxygen after the rapid release of DOX in acidic condition.[53]

In vitro anticancer activity

The cytocompatibility of mPEG-PC was first studied before the *in vitro* anticancer study of DNPs. The cytotoxicity of mPEG-PC against NIH/3T3 and 4T1 cells were studied by an MTT assay. As shown in Fig. S11, mPEG-PC showed low cytotoxicity and the viability of NIH/3T3 cells was more than 80% even at a high polymer concentration of 50 μg/mL. In addition, similar results were obtained when cells were treated with mPEG-PC and light irradiation, suggesting that mPEG-PC had no phototoxicity.

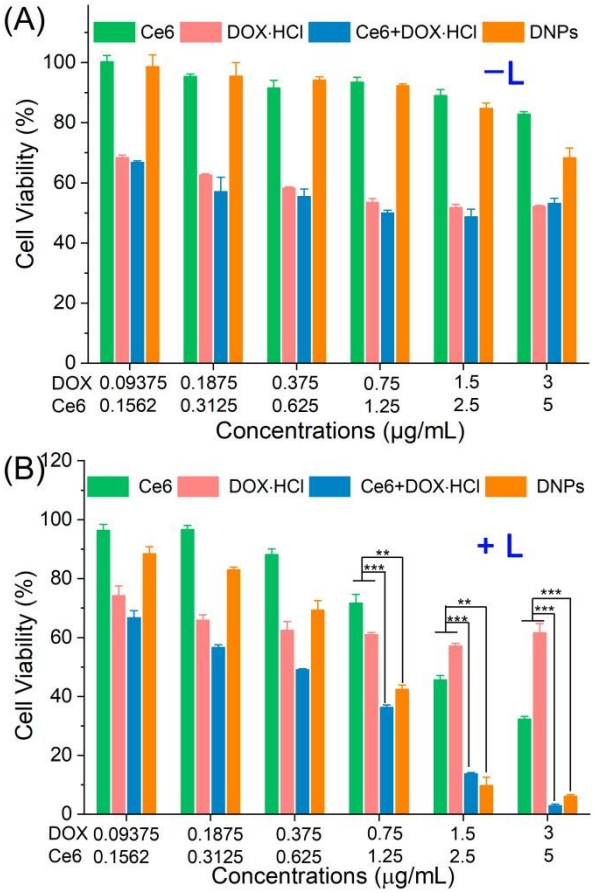

Fig. 4 The cytotoxicity of Ce6, DOX·HCl, the physical mixture of Ce6 and DOX·HCl (Ce6+ DOX·HCl), and DNPs against 4T1 cells after a 24 h incubation without (A) and with (B) light irradiation of 660 nm for 30 s. (n = 3, ** p < 0.01, *** p < 0.001.).

The *in vitro* anticancer activity of DNPs in 4T1 cells with and without light irradiation were then studied; DOX·HCl, Ce6 and their physical mixture (Ce6+DOX·HCl) were used as control groups. As shown in Fig. 4, cells treated with DOX·HCl showed negligible cytotoxicity differences with and without light irradiation because DOX·HCl is not a photosensitizer. In contrast, Ce6 showed the least dark cytotoxicity yet significantly enhanced anticancer efficacy under light irradiation. For example, the viability of 4T1 cells treated with 5 μg/mL Ce6 with and without light irradiation was 32.4% and 83.0%, respectively. Ce6+DOX·HCl and DNPs showed comparable anticancer activity in the dark. When under irradiation, DNPs and Ce6+DOX·HCl showed better anticancer activity than the other two groups, suggesting synergistic anticancer effect of Ce6 and DOX. Furthermore, combination index (CI) values of PDT and chemotherapy in DNPs were calculated and summarized in Table S2. The results (CI < 1) demonstrated that DNPs performed excellent synergistic effect on the inhibition of cancer cell proliferation.

The impact of irradiation time on the anticancer efficacy of DNPs was also studied (Fig. S12). The prolonged irradiation time led to enhanced cancer cell inhibition. The IC_{50}s (Table S3) of DNPs were 9.22, 6.60, and 5.58 μg/mL when the irradiation time was 0.5, 1, and 3 min, respectively. The longer irradiation time could generate more ROS in cancer cells, resulting in more cell damages and better PDT outcomes.

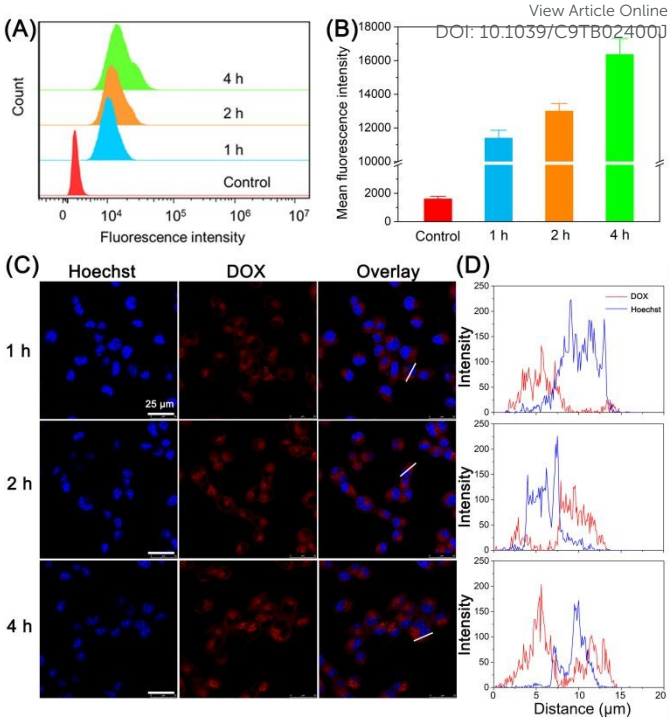

Fig. 5 Flow cytometry (A, B) results of 4T1 cells treated with DNPs for different incubation times in the absence of irradiation.(C) CLSM images and (D) nucleus co-localization analysis of 4T1 cells treated with DNPs for 1, 2, and 4 h.

Light-triggered enhanced cellular uptake and endosomal escape

The cellular uptake behaviors of DNPs by 4T1 cells in the dark were first studied by flow cytometry. 4T1 cells were treated with DNPs for 1, 2, and 4 h. The DNPs showed a time-dependent internalization behavior and the more cellular uptake of DNPs were observed with longer incubation time (Fig. 5A and B). Similar results were observed in the CLSM results (Fig. 5C), and the intracellular co-location analysis (Fig. 5D) showed that some DOX had diffused into nucleus, where DOX can exert the anticancer effect by insertion into DNA. Since polymer nanoparticles are generally internalized by cancer cells in a manner of endocytosis, the acidic environment in endo/lysosomes could trigger the intracellular DOX release of DNPs. As shown in Fig. S13, the co-localization results of DOX and Ce6 indicated that distribution of DOX and Ce6 were not co-localized in the same region, suggesting the intracellular DOX release from DNPs.[54]

We then studied the cellular uptake of DNPs by 4T1 cancer cells under light irradiation. 4T1 cells were cultured with DNPs containing medium and treated with and without light irradiation for 3 min. The cells were then cultured for 2 h to study the impact of light irradiation on the cellular uptake of DNPs. As shown in Fig. (6A and B), a significant increase of intracellular mean fluorescence intensity of Ce6 was observed after light treatment. To explore whether the irradiation accelerated the extracellular release of Ce6 and induced more cellular uptake of Ce6, the *in vitro* release of Ce6 under irradiation was studied (Fig. S14). Obviously, the light irradiation showed negligible effect on the release of Ce6. Therefore, the enhanced cellular uptake of DNPs after light irradiation was ascribed to the Ce6-mediated generation of ROS that induced

lipid peroxidation and thereby improved cell membrane permeability, which was also known as photochemical internalization (PCI).[55, 56]

To verify the ROS generation in PDT, intracellular ROS of 4T1 cells treated with DNPs in the presence and absence of light irradiation was measured by DCFH-DA. DCFH-DA per se has no fluorescence and can pass through cell membrane freely. After internalization, DCFH-DA can be hydrolyzed by esterase to give DCFH that could be oxidized by ROS to give DCF with green fluorescence.[57, 58] The cells were treated with DNPs for 2 h and then irradiated for 3 min. The light irradiation group (+L) showed stronger green fluorescence intensity, confirming the ROS generation after light irradiation (Fig. 6C). It could be observed there was weak DCF fluorescence in the DNPs group without irradiation treatment, which may be ascribed to the endogenous ROS and induction from DOX·HCl.[59, 60] Meanwhile, flow cytometry was employed for a quantitative analysis of the generated ROS (Fig. 6D). The irradiated group presented higher mean fluorescence intensity of DCF, which was consistent with the CLSM result.

Nanoparticles are generally internalized by cancer cells in a manner of endocytosis, after which the nanoparticles could be trapped into acidic endosomes and/or lysosomes.[61] DNPs could accelerate the DOX release in the acidic conditions; however, DOX need to escape from these organelles, diffuse into nucleus, and insert into DNA to exert its anticancer activity. Because ROS could destroy bio-membranes, we then tested whether the organelle membranes could be destroyed after light irradiation (Fig. 6E and F). Obviously, the red fluorescence of DOX and the green fluorescence of lysotracker overlapped to a large extent when cells were treated without irradiation, suggesting that DNPs were mainly in the lysosomes and DNPs were internalized by endocytosis. In contrast, after light irradiation for 0.5 min, the green fluorescence was hardly observed, suggesting that lysosomal membranes were destroyed by ROS generated in PDT. The light-triggered ROS-induced lysosomal membrane damage could boost the endo/lysosomal escape of DNPs and release of DOX, realizing synergistic cancer therapy.

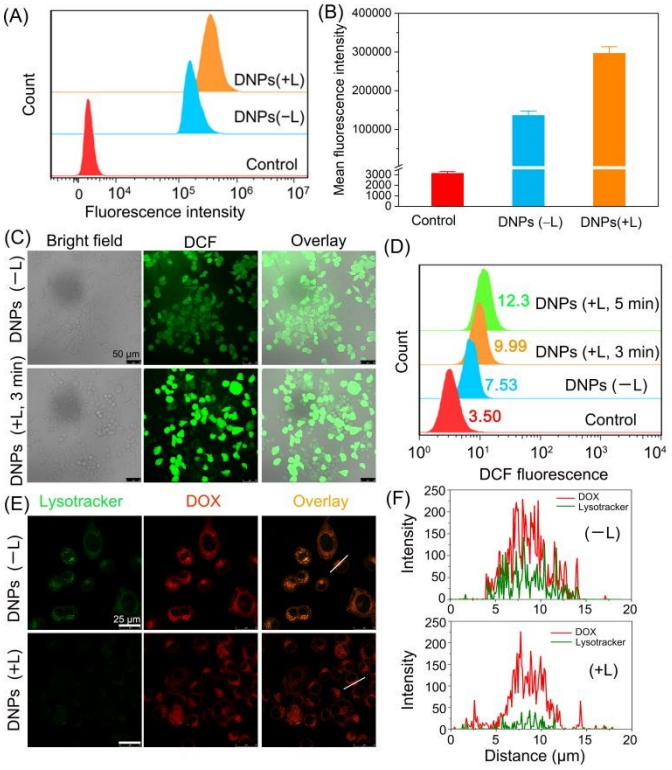

Fig. 6 Flow cytometry analysis (A, B) of DNPs-treated 4T1 cells at 2 h with (+L) and without (-L) the pretreatment of light irradiation for 3 min. (C) CLSM images and (D) flow cytometry analysis for ROS generation of 4T1 cells treated with DNPs with (+L) and without light irradiation (-L). (E) CLSM images and (F) lysosomal co-localization analysis of 4T1 cells incubated with DNPs with (+L) and without light irradiation (-L).

Biodistribution and in vivo antitumor efficacy of DNPs

Encouraged by the *in vitro* synergistic anticancer effect, the *in vivo* biodistribution of DNPs was investigated by *ex vivo* fluorescence imaging. 4T1 tumor-bearing mice were divided into two groups and intravenously injected with DNPs and the physical mixture of Ce6 and DOX·HCl (Ce6+DOX·HCl). The main organs and tumors of mice were collected at desired time points (6 and 24 h) and the fluorescence images were show in Fig. 7A. Tumor in DNPs group showed significantly enhanced fluorescence intensity relative to that of Ce6+DOX·HCl group at 6 h, suggesting the improved accumulation of DNPs by enhanced permeation and retention (EPR) effect.[62] Meanwhile, strong DOX fluorescence was also observed in the kidneys in the DNPs group at 6 h, implying that DNPs were probably cleared by kidney.

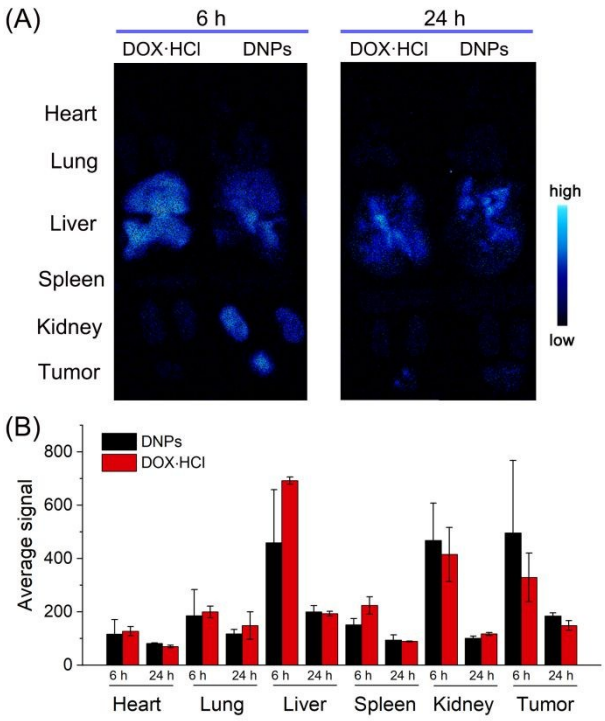

Fig. 7 *Ex vivo* FL images (A) and average signal (B) of main organs and tumors after intravenous injection of DNPs and DOX·HCl.

DOI: 10.1039/C9TB02491

The *in vivo* antitumor efficacy of DNPs was explored on 4T1 tumor-bearing mice. When tumor volume reached 100-150 mm^3, different formulations (Saline, DOX·HCl, Ce6, and DNPs) were administrated via intravenous injection. The tumors of mice in groups of Ce6 and DNPs were further irradiated by 660 nm laser. As shown in Fig. 8, DOX·HCl group showed poor tumor inhibition because of the low DOX dosage (3 mg/kg) than normal one (5 mg/kg). [63, 64] The Ce6 group efficiently suppressed the tumor growth in the first 8 days; however, the tumor volumes rapidly increased one PDT was ceased on day 6. DNPs showed a significantly enhanced tumor inhibition relative to these two groups, indicating that the combinational chemo-photodynamic therapy was superior to monotherapy. The relative tumor volumes of Ce6, DOX·HCl, and DNPs groups on day 12 were 6.64, 6.95, and 4.51 times of the corresponding average tumor volumes on day 0. Meanwhile, the body weights of mice were monitored for preliminary safety evaluation. There were no obvious body weight changes in all groups during the short-term treatment. Hematoxylin and eosin (H&E) assays were further carried out to confirm the antitumor efficacy and organ toxicity. As presented in Fig. S15, DNPs showed negligence damage to the normal organs. No obvious body loss and cardiomyopathy was observed in the DOX·HCl group, which was probably due to the low DOX dose of 3 mg/kg.

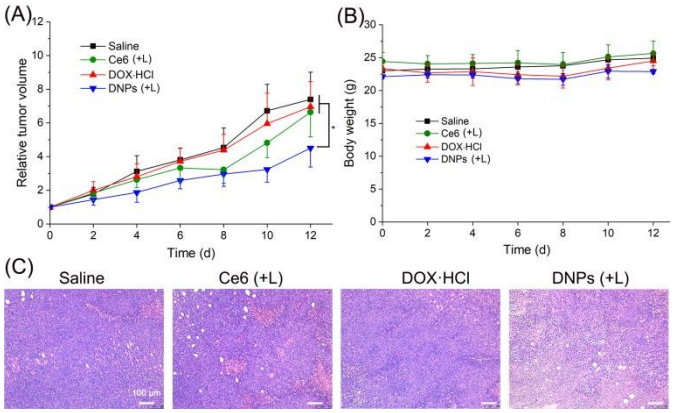

Fig. 8 Tumor growth (A) and body weight changes (B) of 4T1 tumor-bearing Balb/c mice. The tumors of mice in Ce6 and DNPs groups were treated with laser irradiation at 660 nm for 10 min. (C) Images of tumor slices stained with H&E after treatment.

Conclusions

In summary, we reported a strategy of using polycationic polymers to discriminatively load oppositely-charged photosensitizer Ce6 and anticancer drug DOX. The as-prepared co-loaded nanoparticles showed excellent stability and higher encapsulation efficiency of Ce6 owing to the electrostatic attraction between polycationic polymer and anionic Ce6. In addition, DOX and Ce6 showed different release behaviors in weakly acidic condition owing to the different solubilities and interaction forces with polymer matrix, which is conductive to intracellular sequential release of some drug combinations. The DOX and Ce6-coloaded nanoparticles showed *in vitro* synergistic inhibition of 4T1 cancer cells by PCI-mediated enhanced cellular uptake, pH-responsive intracellular DOX release, and efficient endo/lysosome escape of nanoparticles mediated by irradiation-induced ROS. *In vivo* study showed that nanoparticles-based chemo-photodynamic combination therapy had better antitumor efficacy than monotherapy. Our study provided a strategy of using polycationic polymer for differential encapsulation and release of oppositely-charged payloads, which could have great potential in various combination therapies.

Conflicts of interest

There are no conflicts to declare.

Acknowledgements

The authors thank for the financial support of National Natural Science Foundation of China (No. 51903172, 51773130 and 51573111), Sichuan Science and Technology Program (2019YJ0051), and Fundamental Research Funds for the Central Universities (YJ201764). We would like to thank the Analytical & Testing Center of Sichuan University for NMR and TEM tests.

Notes and references

1. B. A. Chabner and T. G. Roberts Jr, *Nature Reviews Cancer*, 2005, **5**, 65.
2. L. Cheng, C. Wang, L. Feng, K. Yang and Z. Liu, *Chem. Rev.*, 2014, **114**, 10869-10939.
3. D. E. Dolmans, D. Fukumura and R. K. Jain, *Nat. Rev. Cancer*, 2003, **3**, 380-387.
4. W. Fan, B. Yung, P. Huang and X. Chen, *Chemical reviews*, 2017, **117**, 13566-13638.
5. X. Deng, Y. Liang, X. Peng, T. Su, S. Luo, J. Cao, Z. Gu and B. He, *Chem. Commun.*, 2015, **51**, 4271-4274.
6. L. Xu, M. Zhao, Y. Yang, Y. Liang, C. Sun, W. Gao, S. Li, B. He and Y. Pu, *J. Mater. Chem. B*, 2017, **5**, 9157-9164.
7. B. Pelaz, C. Alexiou, R. A. Alvarez-Puebla, et al. *ACS Nano*, 2017, **11**, 2313-2381.
8. J. Shi, P. W. Kantoff, R. Wooster and O. C. Farokhzad, *Nat. Rev. Cancer*, 2017, **17**, 20-37.
9. P. Huang, D. Wang, Y. Su, W. Huang, Y. Zhou, D. Cui, X. Zhu and D. Yan, *J. Am. Chem. Soc.*, 2014, **136**, 11748-11756.
10. N. Li, H. Cai, L. Jiang, J. Hu, A. Bains, J. Hu, Q. Gong, K. Luo and Z. Gu, *ACS Appl. Mater. Interfaces*, 2017, **9**, 6865-6877.
11. Y. Liang, W. Gao, X. Peng, X. Deng, C. Sun, H. Wu and B. He, *Biomaterials*, 2016, **100**, 76-90.
12. X. Guo, X. Wei, Z. Chen, X. Zhang, G. Yang and S. Zhou, *Prog. Mater Sci.*, 2020, **107**, 100599.
13. G. Saravanakumar, J. Lee, J. Kim and W. J. Kim, *Chem. Commun.*, 2015, **51**, 9995-9998.
14. D. Hu, L. Chen, Y. Qu, J. Peng, B. Chu, K. Shi, Y. Hao, L. Zhong, M. Wang and Z. Qian, *Theranostics*, 2018, **8**, 1558-1574.
15. Z. Cao, Y. Ma, C. Sun, Z. Lu, Z. Yao, J. Wang, D. Li, Y. Yuan and X. Yang, *Chem. Mater.*, 2018, **30**, 517-525.
16. G. Saravanakumar, H. Park, J. Kim, D. Park, S. Pramanick, D. H. Kim and W. J. Kim, *Biomacromolecules*, 2018, **19**, 2202-2213.
17. L. Yu, Y. Yang, F.-S. Du and Z.-C. Li, *Biomacromolecules*, 2018, **19**, 2182-2193.

18. Y. Chen, Y. Gao, Y. Li, K. Wang and J. Zhu, *J. Mater. Chem. B*, 2019, **7**, 460-468.
19. R. Zhang, R. Xing, T. Jiao, K. Ma, C. Chen, G. Ma and X. Yan, *ACS Appl. Mater. Interfaces*, 2016, **8**, 13262-13269.
20. M. Zasloff, *Nature*, 2002, **415**, 389-395.
21. P. Li, Y. F. Poon, W. Li, H.-Y. Zhu, S. H. Yeap, Y. Cao, X. Qi, C. Zhou, M. Lamrani and R. W. Beuerman, *Nat. Mater.*, 2011, **10**, 149-156.
22. P. Li, C. Zhou, S. Rayatpisheh, K. Ye, Y. F. Poon, P. T. Hammond, H. Duan and M. B. Chan-Park, *Adv. Mater.*, 2012, **24**, 4130-4137.
23. K. Kuroda and W. F. DeGrado, *J. Am. Chem. Soc.*, 2005, **127**, 4128-4129.
24. Y. Pu, Z. Hou, M. M. Khin, R. Zamudio-Vázquez, K. L. Poon, H. Duan and M. B. Chan-Park, *Biomacromolecules*, 2017, **18**, 44-55.
25. W. Chin, C. Yang, V. W. L. Ng, Y. Huang, J. Cheng, Y. W. Tong, D. J. Coady, W. Fan, J. L. Hedrick and Y. Y. Yang, *Macromolecules*, 2013, **46**, 8797-8807.
26. V. W. L. Ng, J. P. K. Tan, J. Leong, Z. X. Voo, J. L. Hedrick and Y. Y. Yang, *Macromolecules*, 2014, **47**, 1285-1291.
27. S. J. Lam, N. M. O'Brien-Simpson, N. Pantarat, A. Sulistio, E. H. Wong, Y. Y. Chen, J. C. Lenzo, J. A. Holden, A. Blencowe, E. C. Reynolds and G. G. Qiao, *Nat. Microbiol.*, 2016, **1**, 16162.
28. Y. Pu, Y. Du, M. M. Khin, V. Ravikumar, S. A. Rice, H. Duan and M. B. Chan-Park, *Macromol. Rapid Commun.*, 2017, **38**, 1600601.
29. Y.-F. Chen, Y.-D. Lai, C.-H. Chang, Y.-C. Tsai, C.-C. Tang and J.-S. Jan, *Nanoscale*, 2019, **11**, 11696-11708.
30. R. Liu, X. Chen, S. P. Falk, K. S. Masters, B. Weisblum and S. H. Gellman, *J. Am. Chem. Soc.*, 2015, **137**, 2183-2186.
31. R. Liu, X. Chen, S. Chakraborty, J. J. Lemke, Z. Hayouka, C. Chow, R. A. Welch, B. Weisblum, K. S. Masters and S. H. Gellman, *J. Am. Chem. Soc.*, 2014, **136**, 4410-4418.
32. D. W. Pack, A. S. Hoffman, S. Pun and P. S. Stayton, *Nat. Rev. Drug Discov.*, 2005, **4**, 581-593.
33. D. He and E. Wagner, *Macromol. Biosci.*, 2015, **15**, 600-612.
34. A. Harada and K. Kataoka, *Macromolecules*, 1995, **28**, 5294-5299.
35. M. Naito, T. Ishii, A. Matsumoto, K. Miyata, Y. Miyahara and K. Kataoka, *Angew. Chem. Int. Ed.*, 2012, **51**, 10751-10755.
36. Y. Lee, T. Ishii, H. Cabral, H. J. Kim, J.-H. Seo, N. Nishiyama, H. Oshima, K. Osada and K. Kataoka, *Angew. Chem. Int. Ed.*, 2009, **48**, 5309-5312.
37. G.-D. Zhang, A. Harada, N. Nishiyama, D.-L. Jiang, H. Koyama, T. Aida and K. Kataoka, *J. Control. Release*, 2003, **93**, 141-150.
38. L. Xu, Y. Yang, M. Zhao, W. Gao, H. Zhang, S. Li, B. He and Y. Pu, *J. Mater. Chem. B*, 2018, **6**, 1076-1084.
39. J. Wei, H. Meng, B. Guo, Z. Zhong and F. Meng, *Biomacromolecules*, 2018, **19**, 2294-2301.
40. X. Peng, Q. Pan, B. Zhang, S. Wan, S. Li, K. Luo, Y. Pu and B. He, *Biomacromolecules*, 2019, **20**, 2372-2383.
41. X. Hu, X. Chen, Z. Xie, S. Liu and X. Jing, *J. Polym. Sci., Part A: Polym. Chem.*, 2007, **45**, 5518-5528.
42. T. Su, F. Cheng, J. Yan, J. Cao, K. Luo, Y. Pu and B. He, *J. Mater. Chem. B*, 2018, **6**, 4687-4696.
43. L. Su, R. Li, S. Khan, R. Clanton, F. Zhang, Y.-N. Lin, Y. Song, H. Wang, J. Fan, S. Hernandez, A. S. Butters, G. Akabani, R. MacLoughlin, J. Smolen and K. L. Wooley, *J. Am. Chem. Soc.*, 2018, **140**, 1438-1446.
44. Z. Guo, K. Zhao, R. Liu, X. Guo, B. He, J. Yan and J. Ren, *J. Mater. Chem. B*, 2019, **7**, 334-345.
45. Y. Pu, L. Zhang, H. Zheng, B. He and Z. Gu, *Polym. Chem.*, 2014, **5**, 463-470.
46. Y. Wang, G. Wei, X. Zhang, X. Huang, J. Zhao, X. Guo and S. Zhou, *Small*, 2018, **14**, 1702994.
47. Y. Zhang, F. Huang, C. Ren, L. Yang, J. Liu, Z. Cheng, L. Chu and J. Liu, *ACS Appl. Mater. Interfaces*, 2017, **9**, 13016-13028.
48. L. Yu, Y. Yang, F. S. Du and Z. C. Li, *Biomacromolecules*, 2018, **19**, 2182-2193.
49. Z. Li, M. Wu, H. Bai, X. Liu and G. Tang, *Chem. Commun.*, 2018, **54**, 13127-13130.
50. X. Yang, B. Zhu, T. Dong, P. Pan, X. Shuai and Y. Inoue, *Macromol. Biosci.*, 2008, **8**, 1116-1125.
51. H. Cabral, Y. Matsumoto, K. Mizuno, Q. Chen, M. Murakami, M. Kimura, Y. Terada, M. R. Kano, K. Miyazono, M. Uesaka, N. Nishiyama and K. Kataoka, *Nat. Nanotechnol.*, 2011, **6**, 815-823.
52. Q. Pan, Z. Zong, J. Shen, H. Xue and Y. Pu, *J. Macromol. Sci., Part A: Pure Appl.Chem.*, 2018, **55**, 691-697.
53. S. Zhong, C. Chen, G. Yang, Y. Zhu, H. Cao, B. Xu, Y. Luo, Y. Gao and W. Zhang, *ACS Appl. Mater. Interfaces*, 2019, **11**, 33697-33705.
54. J. Zhu, C. Chu, D. Li, X. Pang, H. Zheng, J. Wang, Y. Shi, Y. Zhang, Y. Cheng, E. Ren, J. Cheng, X. Chen and G. Liu, *Adv. Funct. Mater.*, 2019, **29**, 1904056.
55. H.-L. Tu, Y.-S. Lin, H.-Y. Lin, Y. Hung, L.-W. Lo, Y.-F. Chen and C.-Y. Mou, *Adv. Mater.*, 2009, **21**, 172-177.
56. Y. Wang, G. Wei, X. Zhang, F. Xu, X. Xiong and S. Zhou, *Adv. Mater.*, 2017, **29**, 1605357.
57. L. Xu, M. Zhao, H. Zhang, W. Gao, Z. Guo, X. Zhang, J. Zhang, J. Cao, Y. Pu and B. He, *Biomacromolecules*, 2018, **19**, 4658-4667.
58. Q. Pan, B. Zhang, X. Peng, S. Wan, K. Luo, W. Gao, Y. Pu and B. He, *Chem. Commun.*, 2019, **55**, 13896-13899.
59. S. Zhang, X. Liu, T. Bawa-Khalfe, L.-S. Lu, Y. L. Lyu, L. F. Liu and E. T. H. Yeh, *Nat. Med.*, 2012, **18**, 1639.
60. P. K. Singal and N. Iliskovic, *N. Engl. J. Med.*, 1998, **339**, 900-905.
61. T.-G. Iversen, T. Skotland and K. Sandvig, *Nano Today*, 2011, **6**, 176-185.
62. T. Wang, D. Wang, J. Liu, B. Feng, F. Zhou, H. Zhang, L. Zhou, Q. Yin, Z. Zhang, Z. Cao, H. Yu and Y. Li, *Nano Lett.*, 2017, **17**, 5429-5436.
63. Y. Pu, S. Chang, H. Yuan, G. Wang, B. He and Z. Gu, *Biomaterials*, 2013, **34**, 3658-3666.
64. Y. Zhang, C. Yang, W. Wang, J. Liu, Q. Liu, F. Huang, L. Chu, H. Gao, C. Li, D. Kong, Q. Liu and J. Liu, *Sci. Rep.*, 2016, **6**, 21225.

View Article Online
DOI: 10.1039/C9TB02400J

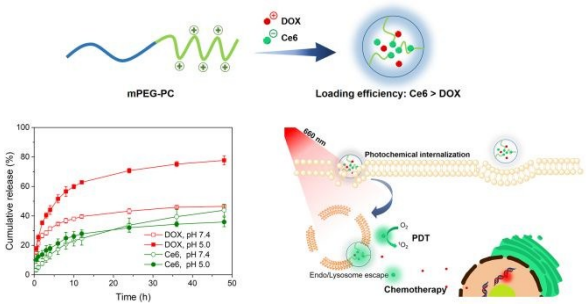

We reported a strategy of using polycationic polymer to realize distinct loading and release of oppositely-charged payloads and a combination therapy.